Stability Analysis of the Overhanging Slopes

Marteen Pratama[1], Thanh Vo[2,*], Adrian Russell[3]

1 Graduate Student, School of Civil and Environmental Engineering, The University of New South Wales, Sydney, Australia.

2 Research Associate, Centre for Infrastructure Engineering and Safety, School of Civil and Environmental Engineering, The University of New South Wales, Sydney, Australia.

3 Associate Professor, Centre for Infrastructure Engineering and Safety, School of Civil and Environmental Engineering, The University of New South Wales, Sydney, Australia

**Author to receive correspondence*

thanh.vo@unsw.edu.au

Abstract

Overhanging slopes have been reported following riverbanks and coastal headland failures. The stability of overhanging slopes is of practical interests and has been investigated in physical tests and numerical models. The geometry of an overhang is an input into most slope stability analysis and is frequently idealised or back-calculated from observed data. Only limited studies have considered the relationship between the geometry and the unsaturated shear strength inherent in the overhanging soil slopes.

This study investigates the geometries of overhanging slopes, which exist while in limiting condition satisfying static equilibrium with soil strength governed by the Mohr-Coulomb failure criterion. The overhanging contour is formulated as the unknown in a boundary value problem and solved for using the slip line theory. Subsequently, results from the dimensionless charts were dimensionalised and analysed by the finite element method to evaluate the influence of flow rule, tension crack layer height and unsaturated shear strength on the stability of overhang.

The solutions are presented in general dimensionless charts. The results show that the curvature of an overhang becomes more pronounced for small values of φ'. It is also demonstrated that changing the contribution of suction to effective stress has a direct impact on the size of an unsaturated soil overhang.

It was found that toppling is the likely failure mechanism of overhang in this study. The presence of a tension crack layer above the arch is required to stabilise an overhanging slope, alongside precise combinations of soil parameters and slope geometry. The influence of flow rule on the factor of safety was small. Varying the tension crack layer thickness to between 0.3 and 0.7 of the overhanging height does not significantly impact the safety factor of the particular slopes considered.

1 INTRODUCTION

Overhanging slopes have been reported in many riverbanks and coastal headlands. Erosion process causes failures of the soil wall with cohesive material on the top and granular material below, and the remnant of which can form an overhanging slope. The stability of overhanging soil slope is of practical interest and has been investigated by physical and numerical modelling using the limit equilibrium method (e.g. Thorne & Tovey, 1981; Van Eerdt, 1985; Pizzuto, 1987; Thorne & Abt, 1993; Darby & Thorne, 1996; Abam, 1997; Rinaldi et al., 2004; Rinaldi & Darby, 2008; Samadi et al., 2011; Samadi et al., 2013; Patsinghasanee et al., 2018). Most of the overhanging slopes are located above the water table where soil can be unsaturated.

Thorne & Tovey (1981) identified three failure mechanisms that govern the stability of overhanging slope: shear, beam and tensile failures. Thorne & Tovey (1981), Van Eerdt (1985), Abam (1997), Samadi et al. (2013), Zhang et al. (2016) and Patsinghasanee et al. (2018) found that beam failure was the controlling mechanism of overhang stability. Equations were proposed for estimating the safety factor of shear and beam failures, and accounting for the stability of cohesive overhang (Samadi et al., 2011; Samadi et al., 2013; Patsinghasanee et al., 2018). Sokolovskii (1965) and Vo & Russell (2019) showed that overhanging slope is more susceptible to toppling failure.

The stability of an overhang is governed by many factors such as geometry, type of material layers, presence of tension cracks, hydraulic confining pressure, soil shear strength, and suction in an unsaturated soil. Quinlan (1987) discussed the work of Jennings (1966) and Lobban which shows that soil with high cohesion favours the development of a small, flat arch while soil with low cohesion favours the development of a much wider and higher arch. The wetting of soil causes a reduction in cohesion and changes in the arch geometry due to soil spalling from the wall. The overhang is stable until being adequately disturbed by environmental changes in and around the bank soils e.g. a vertical crack occurring during the process may extend and eventually cause a toppling type of failure.

Most stability studies considered the slope geometry as an input. This study develops the overhang geometry by imposing a boundary condition requiring the slope contour to coincide with the major principal stress direction. Thorne & Tovey (1981) and Abam (1997) considered the importance of tension crack layer for overhang stability. This study incorporates the tension crack layer into the slope geometry. The surcharge load is assumed equal to the weight of the tension crack layer.

Sokolovskii (1965) and Karaulov & Korolev (2012) developed dimensionless charts of overhanging slope comprised of dry soil using the slip line theory. Vo & Russell (2019) and this study examines dimensionless overhanging charts for soil in a more general condition. The soil is being treated as unsaturated, which has a suction that increases the particle contact forces and thus effective stress. The soil is defined by constant friction angle and a linear variation of cohesion and the contribution of suction to the effective stress with depth. The analysis produces a series of dimensionless charts showing the shapes of overhanging slopes for the case when the soil is at a limiting condition. Numerical analysis of the overhanging slope is carried out using the software *Plaxis* (Plaxis, 2019) to investigate the influence of flow rule and the tension crack layer height on slope failure.

2 GOVERNING EQUATIONS AND BOUNDARY CONDITIONS

2.1 Governing Equations

The soil shear strength of overhanging slope is governed by Mohr-Coulomb failure criterion:

$$\tau = c' + \sigma' \tan\varphi' \quad (1)$$

where c' is cohesion, φ' is internal friction angle, and σ' is the effective stress, defined by Bishop (1959) for unsaturated soil condition as:

$$\sigma' = \sigma - u_a + \chi(u_a - u_w) \quad (2)$$

where σ is total stress, χ is the effective stress parameter, u_a is the pore air pressure, and u_w is the pore water pressure. The value of χ and thus σ' have been studied by many (e.g Khalili & Khabbaz, 1998; Khalili et al., 2008).

For simplicity, φ' is assumed to be constant, c' and χs are assumed to vary linearly with depth z according to:

$$c' = c'_0 + k_c z \quad (3)$$

$$\chi s = (\chi s)_0 + k_{\chi s} z \quad (4)$$

where c'_0 is cohesion at z=0, $(\chi s)_0$ is the contribution of suction to the effective stress at z=0 and k_c, $k_{\chi s}$ are constants.

The static equilibrium equations (x and z are horizontal and vertical axis, respectively) can be expressed as:

$$\frac{\partial \sigma_{xx}}{\partial x} + \frac{\partial \sigma_{xz}}{\partial z} = 0 \quad (5)$$

$$\frac{\partial \sigma_{xz}}{\partial x} + \frac{\partial \sigma_{zz}}{\partial z} = \gamma \quad (6)$$

where σ_{zx} is the shear stress and γ is the total unit weight of soil, and σ_{xx}, σ_{zz} are normal stresses in the x and z directions, respectively.

At the onset of failure defined by the Mohr-Coulomb criterion the stress components σ_{zz}, σ_{xx}, σ_{zx} satisfy:

$$\sigma_{zz} = [(1 + \sin\varphi' \cos 2\psi)\sigma'_m - c' \cot\varphi'] - \chi s \quad (7)$$

$$\sigma_{xx} = [(1 - \sin\varphi' \cos 2\psi)\sigma'_m - c' \cot\varphi'] - \chi s \quad (8)$$

$$\sigma_{zx} = \sigma'_m \sin\varphi' \sin 2\psi \quad (9)$$

where ψ is the angle between the major principal stress direction and the vertical axis and σ'_m is effective mean stress.

Following the approach from Vo and Russell (2017), the stress quantities in Eqs. (5) – (9) are scaled by S and the length quantities are scaled by L, the slip line governing equations can be written in the following dimensionless form:

$$\langle\eta\rangle \equiv \begin{cases} d\hat{x} = \tan(\psi + \mu) d\hat{z} \\ d\widehat{\sigma'_m} + 2\tan\varphi' \widehat{\sigma'_m} d\psi = F(d\hat{z} - \tan\varphi' \, d\hat{x}) \end{cases} \quad (10)$$

$$\langle\xi\rangle \equiv \begin{cases} d\hat{x} = \tan(\psi - \mu) d\hat{z} \\ d\widehat{\sigma'_m} - 2\tan\varphi' \widehat{\sigma'_m} d\psi = F(d\hat{z} + \tan\varphi' \, d\hat{x}) \end{cases} \quad (11)$$

in which

$$F = \frac{L}{S}\left[\gamma + \frac{\partial(\widehat{c'}\cot\varphi' + \widehat{\chi s})}{\partial \hat{z}}\right] \quad (12)$$

where $\widehat{\sigma'_m} = \frac{\sigma'_m}{S}$, $\widehat{c'} = \frac{c'}{S}$, $\widehat{\chi s} = \frac{\chi s}{S}$, $\mu = \frac{\pi}{4} - \frac{\varphi'}{2}$, $\hat{z} = \frac{z}{L}$, and $\hat{x} = \frac{x}{L}$ are non-dimensional quantities and ξ, η denote families of stress slip lines. It can be observed from Eqs. (10) – (11) that the solutions $(\widehat{\sigma'_m}, \psi, \hat{z}, \hat{x})$ are dependent on $\frac{\partial(\widehat{c'}\cot\varphi' + \widehat{\chi s})}{\partial \hat{z}}$ and φ'. When applied to a boundary value problem a solution $(\widehat{\sigma'_m}, \psi, \hat{z}, \hat{x})$ also depends on boundary conditions. If $S = q_{int} + c'_0 \cot\varphi' + (\chi s)_0$ is adopted, F becomes:

$$F \equiv \frac{L(\gamma + k_c \cot\varphi' + k_{\chi s})}{q_{int} + c'_0 \cot\varphi' + (\chi s)_0} \quad (13)$$

F is a dimensionless parameter. q_{int}=$h\gamma$ denotes the stress applied on the soil surface due to the height of tension crack layer h (Fig. 1).

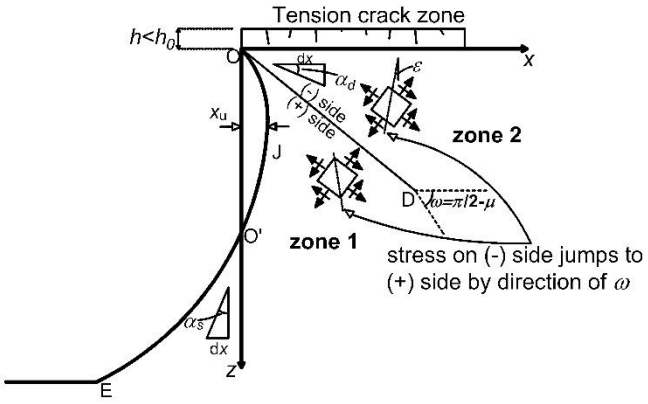

Figure 1. Stress acts on the two sides of an admisible discontinuity (after Vo & Russell, 2019).

2.2 Boundary Conditions

2.2.1 On the (+) side of OD (Fig. 1)

The stress jump across the discontinuity is illustrated in Fig. 1. The effective mean stress at depth z is $\frac{h\gamma + z\gamma + c'\cot\varphi' + \chi s}{1 + \sin\varphi'}$ on the (-) side of the discontinuity (in zone 2). On the (+) side of the discontinuity, the effective mean stress is:

$$\sigma'_m += \left(\frac{h\gamma + z\gamma + c'\cot\varphi' + \chi s}{1 + \sin\varphi'}\right)\frac{\sin(\Delta + \delta')}{\sin(\Delta - \delta')} \quad (14)$$

where δ' and Δ are defined as in Vo and Russell (2019) and $\sin\Delta = \frac{\sin\delta'}{\sin\varphi'}$.

The second boundary condition is given from the discontinuity trajectory (Fig. 1):

$$\frac{dz}{dx} = \tan\alpha_d \quad (15)$$

where α_d is the gradient of the discontinuity trajectory and $\alpha_d = \frac{1}{2}(\Delta + \delta')$.

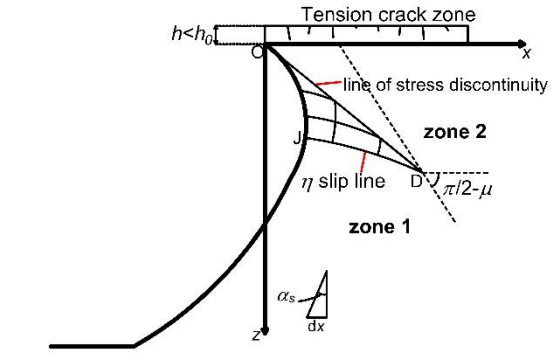

Figure 2. Overhanging slope geometry formation with slip line theory (after Vo & Russell, 2019).

Across the stress discontinuity, the effective major principal stress direction jumps by an angle ω. It can be found from that the third boundary condition is given by:

$$\psi_d = (\pi/2 - \Delta) \quad (16)$$

2.2.2 Along the slope surface

The effective mean stress along the slope surface is:

$$\sigma'_{\mathrm{m}} = \frac{c' \cot \varphi' + \chi s}{1 - \sin \varphi'} \quad (17)$$

The second and third boundary conditions can be found from the curvature of the slope (Fig. 1):

$$\frac{\mathrm{d}x}{\mathrm{d}z} = \tan \alpha_{\mathrm{s}} \quad (18)$$

$$\psi_{\mathrm{s}} = \alpha_{\mathrm{s}} \quad (19)$$

2.2.3 At point O

z=0 at point O so Eq. (13) gives:

$$\sigma'_{\mathrm{m}} += \left[\frac{q_{\mathrm{int}} + c'_0 \cot \varphi' + (\chi s)_0}{1 + \sin \varphi'}\right] \frac{\sin(\Delta + \delta')}{\sin(\Delta - \delta')} \quad (20)$$

The mean stress is unique at point O. Equating the stress $\sigma'_{\mathrm{m}}+$ in Eq. (20) to the stress σ'_{m} in Eq. (17) leads to:

$$q_{\mathrm{int}} = [c'_0 \cot \varphi' + (\chi s)_0] \left[\left(\frac{1 + \sin \varphi'}{1 - \sin \varphi'}\right) \frac{\sin(\Delta - \delta')}{\sin(\Delta + \delta')} - 1\right] \quad (21)$$

The direction of the major principal stress is unique at point O. Equating ψ_{s} in Eqs. (19) to ψ_{d} in Eq. (16) leads to:

$$\Delta = \pi/2 - \alpha_{\mathrm{s}} \quad (22)$$

Eqs. (21) and (22) show that there is a corresponding surcharge q_{int} for each value of α_{s} (where α_{s} represents the curvature of the overhanging surface at O). When α_{s}=0 (vertical slope), $\Delta = \frac{\pi}{2} \rightarrow \frac{\sin(\Delta - \delta')}{\sin(\Delta + \delta')} = 1$ and $q_{\mathrm{int}} = [c'_0 \cot \varphi' + (\chi s)_0] \left(\frac{2 \sin \varphi'}{1 - \sin \varphi'}\right) \equiv q_{\mathrm{min}}$ as per Vo & Russell (2017).

3 OVERHANGING SLOPE GEOMETRY

Fig. 1 presents the geometry of the slope containing an overhang, with vertical length OO' and undermining distance x_{u} at certain depth. The overhanging contour OE in Fig. 1 coincides with the direction of the major principal stress and permits the soil to be at limiting equilibrium everywhere. The contour of the slope was initially unknown, it was obtained in Vo and Russell (2019) as part of the solution of the boundary value problem detailed above.

For overhanging slope problem, Sokolovskii (1965), Karaulov & Korolev (2012), and Vo & Russell (2019) assumed the existence of an admissible stress discontinuity OD (Fig. 1). Admissible stress discontinuity is used extensively in rigid-plastic limit analysis and in the slip line theory. Constructing the stress discontinuity is critical to finding a solution.

A tension crack layer, which locates at the upper surface of the slope, is an important consideration for overhang stability (Thorne & Tovey, 1981; Abam, 1997; Patsinghasanee et al., 2018). Vo & Russell (2019) assumed the tension crack layer to form as part of the failure mechanism. They emphasized that the height of the tension crack layer is limited by the following condition:

$$h \leq \frac{(\chi s)_0 (1 - K_a) + 2c'_0 \sqrt{K_a}}{\gamma K_a + k_{\chi s} (K_a - 1) - 2k_c \sqrt{K_a}} = h_0 \quad (23)$$

where h_0 is a bounding height and K_{a} is the Rankine active earth pressure, $K_a = \frac{(1 - \sin \varphi')}{(1 + \sin \varphi')}$.

The overhanging slope contour, i.e the segment OJ in Fig. 2, was built using the slip line theory, where an η slip line passes through the discontinuity line OD at point D and the slope contour OJ at point J. Vo & Russell (2019) presented the slope contour OJ because toppling failure is considered as governing failure mechanism which could occur around point O.

Dimensionless overhang contours were presented in Vo & Russell (2019) for F = 0.01 and φ'= 10°, 20°, 30°, 40°, 50°, 60°, 70°; with α_{s}= 9°, 18°, 27°, 36°, 45°, 54°, 63°, 72°, 81°. Fig. 3 shows examples of overhanging contours for φ'= 20°, 40°. It is shown that for a given φ', when α_{s} increases (or q_{int}=$h\gamma$ decreases), a slope at limiting condition has a more pronounced overhang i.e. a thinner cracked soil layer is balanced by a more pronounced overhang and a thicker cracked soil layer by a steeper overhang (Vo & Russell, 2019). The $\hat{x}$ and $\hat{z}$ axes in the charts are dimensionless and need to be multiplied by L to obtain their corresponding dimensional values.

4 INSIGHTS FROM NUMERICAL ANALYSIS BY PLAXIS

Numerical analyses of overhanging slopes were conducted in *Plaxis*. A factor of safety (FOS) in *Plaxis* was determined using shear strength reduction technique (Matsui & San, 1992; Griffiths & Lane, 1999). The FOS in *Plaxis* is denoted as ΣMsf at failure and defined as:

$$\sum Msf = \frac{\tan \varphi'_{\mathrm{input}}}{\tan \varphi'_{\mathrm{reduced}}} = \frac{c'_{\mathrm{input}}}{c'_{\mathrm{reduced}}} \quad (24)$$

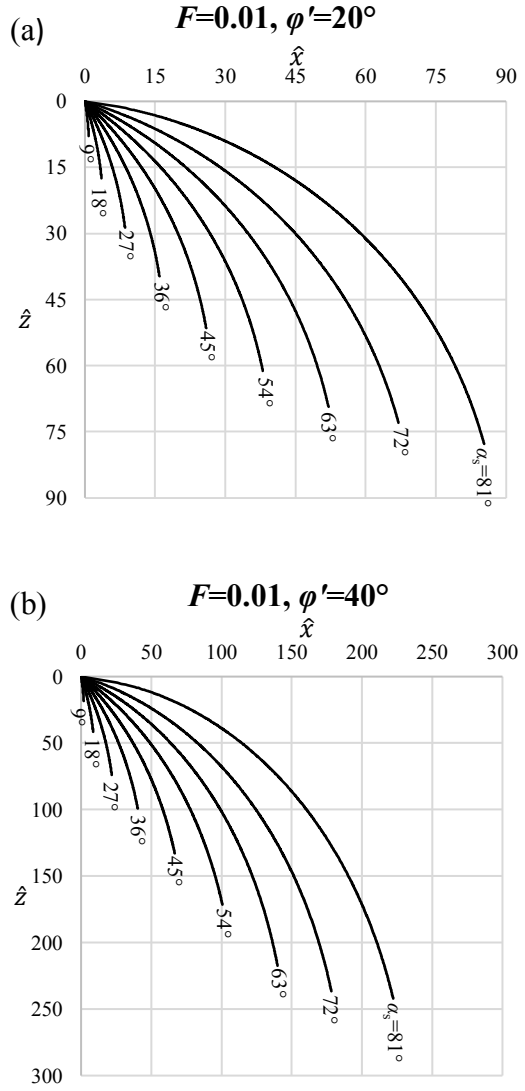

Figure 3. Dimensionless overhanging slope geometry presented by Vo & Russell (2019) for $F = 0.01$, (a) φ'=20°, (b) φ'=40°; presented for α_s= 9°, 18°, 27°, 36°, 45°, 54°, 63°, 72°, 81°.

Vo & Russell (2019) assumed a rigid-plastic stress field in the slip line theory; in reality, part of the overhang may be elastic. The material model in *Plaxis* was assumed to be elastic-plastic Mohr-Coulomb, unsaturated and homogenous i.e $k_{\chi s}$=k_c= 0. Hydraulic confining pressure was not considered. The value of *c'* was set to zero to obtain the critical stability condition (i.e. FOS = 1.0) for different φ'.

The limitation of $h \leq h_0$ was followed when estimating the tension crack layer height. The tension crack layer was modelled as a linear-elastic soil layer. It is noted that the overhanging slope will fail if the tension crack layer is absent during the first construction stage in *Plaxis*. The presence of the tension crack layer or surcharge load above the overhanging slope surface is important for overhang stability.

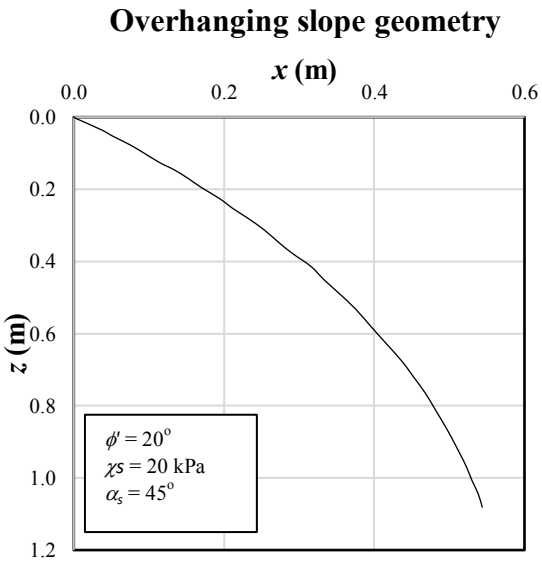

Figure 4. Dimensional geometry of overhanging slope for φ'= 20°, χs = 20 kPa, and α_s = 45°.

A contour from Fig. 3 is now selected to explain the conversion from dimensionless to a dimensional geometry. The length scale L was estimated by choosing values of γ, φ', χs then determining the value of h so that F = 0.01 (Eq. 12). For example, an overhang is considered with γ= 17 kN/m^3, φ' = 20°, c'=0 kPa, χs = 20 kPa, α_s= 45°. From Eq. (23), h_0 = 1.22 m, thus h = 0.9 m can be chosen for this overhang dimension (q_{int} = 15.3 kPa). Keeping the value of F = 0.01, L = 0.021 m is obtained so the dimensional overhang geometry can be constructed as shown in Fig. 4.

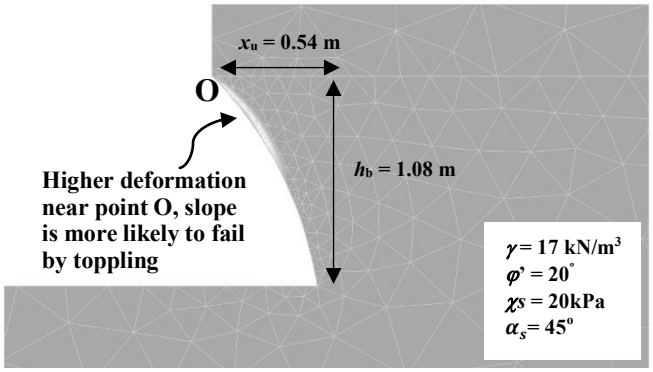

Figure 5. *Plaxis* modelling result shows toppling failure becomes controlling failure mechanism for overhang stability.

Numerical models of overhangs with φ' = 20°, 40° and α_s = 9° to 81° were analysed in *Plaxis*. E'=60,000 kPa and ν'=0.333. Values of h and L were chosen repeatedly until an analysis reaches critical stability (FOS close to 1.0). Example of a critically stable overhanging slope (γ = 17 kN/m^3, φ'= 20°, χs= 20 kPa, and α_s= 45°) is shown in Fig. 5. The undermining distance x_u and the overhanging block height h_b are also shown in Fig. 5.

Results of numerical modelling in *Plaxis* show that toppling failure is likely. For example, in Fig. 5, the area shaded by lighter colours near point O indicates higher deformation compared to the surrounding area shaded by darker colours. Thus soil spalling from the overhang wall near point O is likely and this would eventually lead to a toppling type of failure.

The geometry of a stable overhanging slope is related to soil parameters. Combinations of geometry and soil parameters (γ, φ', χs) can lead to a stable overhang. Determining h would be important to obtain a stable overhang in practice.

Examples are presented in Fig. 6 and Fig. 7 of stable overhanging slopes with $\varphi' = 20°$ and $\alpha_s = 54°$, $\varphi' = 40°$ and $\alpha_s = 72°$, for χs= 5 to 50 kPa. They show that increases in φ', χs are associated with bigger stable overhang geometries.

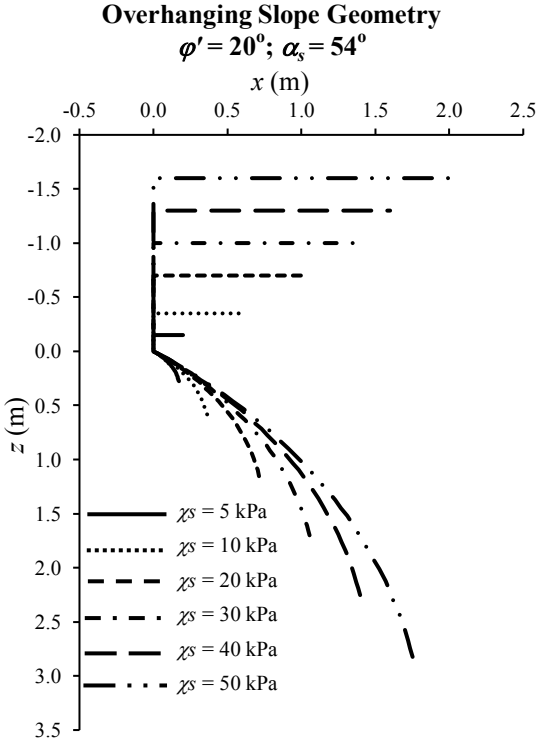

Figure 6. Overhanging slope geometry of at critical stability for $\varphi' = 20°$ and $\alpha_s = 54°$, with χs = 5, 10, 20, 30, 40, and 50 kPa.

Vo & Russell (2019) assumed the soil body to be fully-associated ($\psi' = \varphi'$). $\psi' = 0°$ is adopted here for the non-associated models in *Plaxis*.

One objective of this numerical modelling was to compare soil displacements of models adopting similar geometries and parameters but different flow rules (i.e. the associated versus the non-associated flow rules).

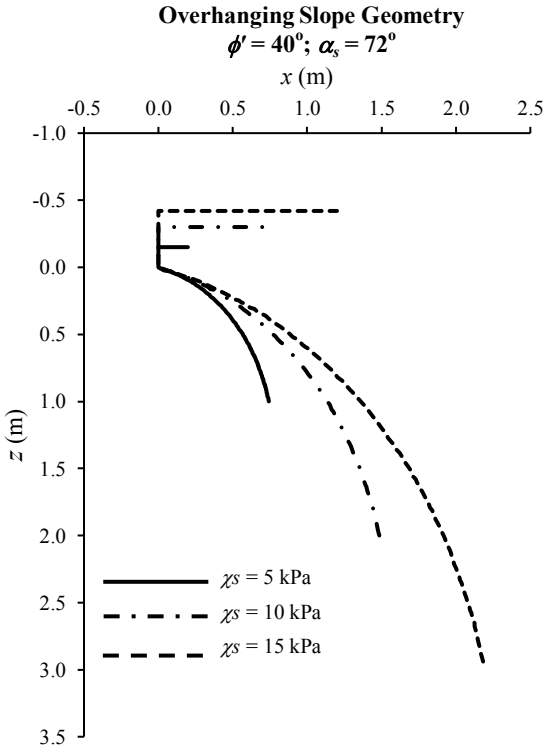

Figure 7. Overhanging slope geometry of at critical stability for $\varphi' = 20°$ and $\alpha_s = 54°$, with χs = 5, 10, 15 kPa.

The maximum horizontal displacements of overhanging slope models with γ = 17 kN/m^3, φ'= 20°, and χs= 5 to 50 kPa for $\alpha_s = 45°$ are obtained from *Plaxis* outputs and plotted in Fig 8. The results show that differences in the maximum horizontal displacements (due to different flow rules applications) become higher when χs increases. Those are between 0.07 to 6.04 mm.

Another objective was to study the range of h that can be applied to stabilise the overhanging slope. Thorne & Abt (1993) suggested h to be half of the overhanging height h_b. They emphasised that the safety factor would not change by more than 10% when the ratio of h/h_b varies between 0.3 and 0.7. To investigate this, numerical models with φ'= 20°, χs= 30 kPa, $\alpha_s = 45°$ were analysed. Table 1 shows that when h ranges between 0.479 m to 1.117 m (the ratio of h/h_b varies from 0.3 to 0.7), the factors of safety vary by no more than 6%.

5 CONCLUSION

This paper presents insights from numerical modelling the overhanging slopes reported by Vo & Russell (2019). Similar to what was reported in that paper, it was found that combinations of soil parameters (unit weight, shear strength, and suction in unsaturated material), slope geometry, and tension crack layer height can lead to a critically stable overhang (i.e. FOS = 1.0). However, additional external loads acting on the soil body

(e.g those due to wind and external water flow) will impact this stability.

Vo & Russell (2019) showed that the geometry of a stable overhang is related to soil parameters. A more pronounced overhang curvature becomes possible for smaller values of φ'. Varying the contribution of suction to effective stress changes the size of a stable overhang.

It was found that the presence of a tension crack layer above the overhang surface is important for stability. The overhang may fail if the slope is unloaded (i.e. the tension crack layer is excluded from the model). Failure will also occur if the surcharge load above the slope is too high.

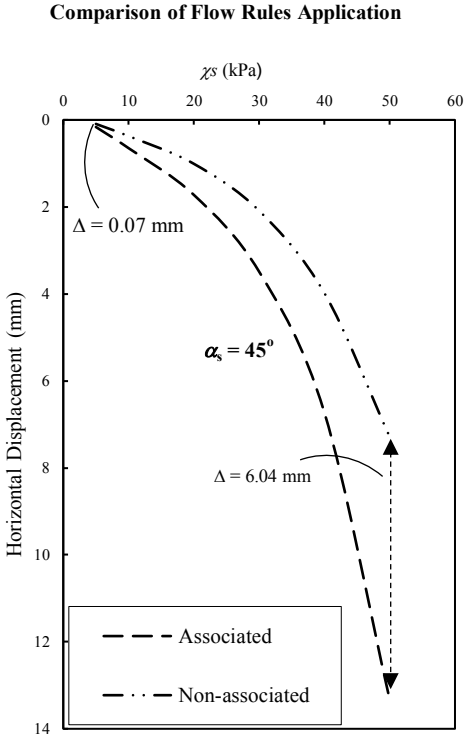

Figure 8. Comparison of maximum horizontal displacements on applications of associated and non-associated flow rules for overhanging slopes with $\varphi' = 20°$, $\alpha_s = 45°$, with $\chi s = 5$ to 50 kPa.

Table 1. Comparison of the safety factors of overhanging slopes when h/h_b ratios vary between 0.3 – 0.7

x_u (m)	h_b (m)	h (m)	h/h_b ratio	Factor of safety
0.803	1.596	0.479	0.3	1.098
0.803	1.596	0.638	0.4	1.091
0.803	1.596	0.798	0.5	1.094
0.803	1.596	0.958	0.6	1.092
0.803	1.596	1.117	0.7	1.097

Vo & Russell (2019) showed that high stresses are concentrated near the top of an overhang causing it to be highly susceptible to toppling. Numerical modelling results also show topppling to be a likely failure mechanism. The area prone to toppling failure is smaller for smaller φ'.

Numerical modelling results show that adopting either the associated or the non-associated flow rules results in small differences in maximum horizontal displacements. Varying the ratio h/h_b (i.e. tension crack layer height to overhanging block height) within a certain range may not impact greatly the factor of safety. For example, for overhanging slopes reconstructed from Vo & Russell (2019) with $\varphi' = 20^o$, when (h/h_b) varies from 0.3 to 0.7, numerical modelling results show that the safety factors vary by no more than 6 %.

6 REFERENCES

Abam, T. K. S. (1997). "*Genesis of channel bank overhangs in the Niger Delta and analysis of mechanisms of failure*". Geomorphology 18(2): 151-164.

Darby, S. E. and Thorne, C. R. (1996). "*Development and testing of riverbank-stability analysis*". Journal of Hydraulic Engineering, 122(8): 443-454.

Griffiths, D. V., and Lane, P. A. (1999). "*Slope stability analysis by finite elements*". Gétechnique, 49(3*)*: 387-403.

Jennings, J. E. (1966). "*Building on dolomites in the Transvaal*". Civil Engineer in South Africa, 8(2), 41-62.

Karaulov, A. and Korolev, K. (2012). "*Approximation of the perimeter of an equally stable unloaded soil slope*". Soil Mechanics and Foundation Engineering, 49(3): 1-6.

Khalili, N., Geiser, F., & Blight, G. E. (2004). "*Effective stress in unsaturated soils: Review with new evidence*". International Journal of Geomechanics*, 4*(2): 115-126.

Khalili, N., Habte, M. A., & Zargarbashi, S. (2008). "*A fully coupled flow deformation model for cyclic analysis of unsaturated soils including hydraulic and mechanical hystereses*". Computers and Geotechnics, 35(6): 872-889.

Patsinghasanee, S., Kimura, I., Shimizu, Y., Nabi, M. (2018). "*Experiments and modelling of cantilever failures for cohesive riverbanks*". Journal of Hydraulic Research, 56(1): 76-95.

Pizzuto, J. E. (1984). "*Bank erodibility of shallow sandbed streams*". Earth Surface Processes and Landforms, 9(2): 113-124.

Plaxis. (2019). "*PLAXIS 2D Reference Manual 2019*". Retrieved 8 April 2019 from https://www.plaxis.com.

Quinlan, J. F. (1987). Discussion of "*The arch in soil arching*" by R. L. Handy. Journal of Geotechnical Engineering*,* 113(3): 272-274.

Rinaldi, M. and Darby, S. E. (2007). "*9 Modelling river-bank-erosion processes and mass failure mechanisms: progress towards fully coupled simulations*". Developments in Earth Surface Processes*,* 11: 213-239.

Rinaldi, M., Casagli, N., Dapporto, S., Gargini, A. (2004). "*Monitoring and modelling of pore water pressure changes and riverbank stability during flow events*". Earth Surface Processes and Landforms, 29(2): 237-254.

Samadi, A., et al. (2011). "*Identifying the effects of parameter uncertainty on the reliability of modelling the stability of overhanging, multi-layered, river banks*". Geomorphology, 134(3-4): 483-498.

Samadi, A., et al. (2013). "*Experimental and numerical investigation of the stability of overhanging riverbanks*". Geomorphology, 184: 1-19.

Sokolovskii, V. V. (1965). "*Statics of soil media*". Pergamon Press: Oxford, UK.

Thorne, C. R. and S. R. Abt (1993). "*Analysis of riverbank instability due to toe scour and lateral erosion*". Earth Surface Processes and Landforms*,* 18(9): 835-843.

Thorne, C. R. and N. K. Tovey (1981). "*Stability of composite river banks*". Earth Surface Processes and Landforms, 6(5): 469-484.

Van Eerdt, M. M. (1985). "Salt marsh cliff stability in the oosterschelde". Earth Surface Processes and Landforms, 10: 95-106.

Vo, T. and A. R. Russell (2017). "*Stability charts for curvilinear slopes in unsaturated soils*". Soils and Foundations*,* 57(4): 543-556.

Vo, T. and Russell, A. R. (2019). "*Contours of saturated and unsaturated overhanging slopes at limiting equilibrium condition*". International Journal for Numerical and Analytical Methods in Geomechanics, 44(1): 93-166.

Zhang, K., Tan, P., Ma, G., & Cao, P. (2016). "*Modeling of the progressive failure of an overhang slope subject to differential weathering in Three Gorges Reservoir, China*". Landslides*,* 13(5): 1303-1313.